Motion of a droplet through microfluidic ratchets

Jing Liu (刘晶), Yit Fatt Yap (叶逸发), and Nam-Trung Nguyen (阮南忠)[*]

School of Mechanical and Aerospace Engineering, Nanyang Technological University, 50 Nanyang Avenue,
Singapore 639798, Singapore

We report numerical and experimental studies on a droplet moving through an array of mirofluidic ratchets. Droplets are formed at a T junction and subsequently forced through microfluidic ratchets in the form of diffuser/nozzle structures. At the same flow rates of the continuous and the dispersed phases, the velocity of the droplet is determined by the viscosity of the continuous phase and the interfacial tension between the two phases. Both numerical and experimental results show that the velocity of the droplet increases with increasing capillary number. The droplet velocity is higher than the mean velocity of the fluid system and increases with increasing viscosity of the continuous phase or decreasing interfacial tension. In all experiments, the droplet moves faster in the diffuser direction than in the nozzle direction. Our findings allow the development of a measurement approach for interfacial tension. The rectification characteristics can be used for the development of micropumps for multiphase systems.

I. INTRODUCTION

In the last decade, the field of microfluidics has been developing rapidly because of its broad applications in biology, chemistry, drug delivery, and medical diagnostics. Droplet-based microfluidics have been used for mixing [1], separation [2], or reaction [3]. Monodisperse droplets were generated using different microfluidic systems such as T junction [4,5], flow focusing [6], and coflowing [7] configurations. The droplet size is controlled by parameters such as flow rate ratio, viscosity, interfacial tension, and temperature [8]. In most droplet-based microfluidic systems, a droplet train is delivered in microchannels with a fixed cross section by external sources such as syringe pumps. However, many important lab-on-a-chip applications require the delivery of droplets in a stand-alone system with integrated pumps. Furthermore, *in situ* measurement of interfacial tension between the two phases of an emulsion with existing droplets is a current challenge, because most of the recent techniques for the measurement of interfacial tension in microscale are based on the formation process of droplets [9,10]. Cabral and Hudson [11] reported a microfluidic instrument to measure interfacial tension based on the deformation and retraction dynamics of droplets under extensional flow. This technique requires an external high-speed camera and an image processing system. A measurement technique based on the characteristics of the motion of a droplet such as its velocity can be easily implemented with optical detection as demonstrated previously [12].

In this paper, we report the behavior of motion of a deformed droplet through microfluidic ratchets. Microfluidic ratchets are asymmetric microchannels called diffuser/nozzle structures. Mineral oil with different surfactant concentrations and de-ionized (DI) water were used as the working liquids. In the numerical investigation, we used level-set method to track the interface movement between the two liquid phases. Simulation and experiments were carried out to investigate how the droplet velocity is affected by flow direction, droplet size, viscosities of the two phases, and their interfacial tension. We show that the motion of a droplet flowing through microfluidic ratchets exhibits rectification behavior and depends on the viscosity of the continuous phase as well as the interfacial tension. This unique behavior opens ways for pumping a droplet train and for measuring interfacial tension in a microfluidic system.

II. DEVICE AND MATERIALS

Figure 1(a) depicts the test device used in our experiments. Two pairs of oil and water ports form two T junctions to generate droplets in both directions of the ratchets. The pressure ports can be used for the measurement of pressure drop across the ratchet array. Another purpose of these ports is their use for the addition of the continuous phase (oil) to accelerate the droplets and to increase their spacing. For instance, the additional oil inlet allows only one droplet to be in the test section under the condition of a lower flow rate ratio between mineral oil and DI water.

The device was fabricated in polydimethylsiloxane (PDMS, Sylgard 184, Dow Corning) using soft lithography. The photomask was designed with AUTOCAD and printed on a 5×5 in.^{2} plastic transparency film with a resolution of 8000 dpi. SU-8 2050 resist was spin coated on a cleaned 4 in. silicon wafer. After a soft bake to harden the SU-8 layer, uv exposure was carried out with transparency mask for 35 s. Developing in isopropanol results in the SU-8 mold for the later PDMS device. The mixture of PDMS and curing agent was then poured over the mold. The thickness of PDMS was kept at approximately 0.5 cm to avoid leakage at the fluidic interconnects in the later experiments. After curing, the PDMS part was peeled from the mold. The six ports depicted in Fig. 1 with 0.75 mm diameter were punched into the PDMS device. The patterned PDMS part and another blank PDMS piece were treated in oxygen plasma for 30 s at a power of 100 W. The two PDMS pieces were subsequently

*mntnguyen@ntu.edu.sg
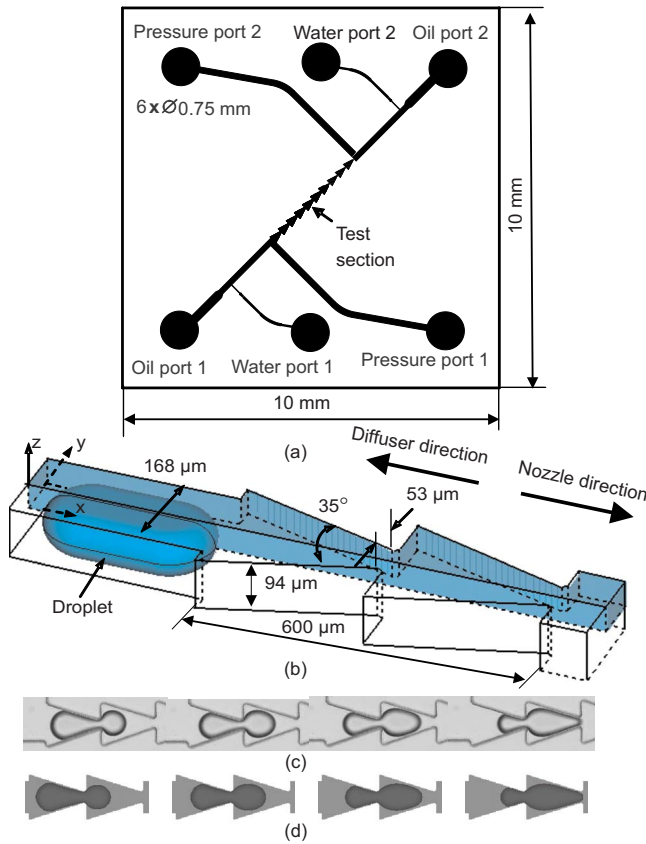
FIG. 1. (Color online) (a) Device schematic for investigation of microdroplets in diffuser/nozzle structures. The test section contains ten diffuser/nozzle structures; (b) numerical model and dimensions of the ratchet; (c) deformation of a droplet passing through the ratchet; (d) simulated deformation of a droplet under the same condition as of the experiment shown in (c).

brought to contact. An additional heat treatment returns the channel surface to a hydrophobic state.

The channel dimension after bonding was measured with a confocal microscopy system. In the past, we have tested these ratchets with different opening angles for continuous single-phase flow [13]. According to this study, an opening angle of 35° exhibits the largest rectification effect. Thus, this opening angle is selected for the current study. Two *T* junctions are used for generating droplets in both directions of the ratchet [Fig. 1(a)]. The directions of diffuser and nozzle are defined in Fig. 1(b). The pressure ports were used for the possible measurement of pressure drop across the test section. The flow rates of the two liquids are adjusted so that only a single droplet can pass through the test section. DI water works as the disperse phase. We used mineral oil (Sigma M5904) as the continuous phase. The oil was mixed with surfactant Span 80 (Sigma S6760) at different concentrations of 0.1% weight by weight (w/w), 0.5% (w/w), and 1.0% (w/w) to control the interfacial tensions. The corresponding interfacial tensions are measured using a commercial tensiometer (FTA 200, First Ten Angstrom, USA) as 6.17, 4.82, and 4.45 mN/m, respectively. The error of the measurement is less than 0.5 mN/m. The viscosities of the oil were measured as 23.8 mPa and do not change significantly with the different surfactant concentrations. Oil and water

are kept in Hamilton glass syringes. Each syringe was driven by an individual syringe pump (KDS 230, KD Scientific Inc., USA) to provide the different flow rates. A high-speed camera (FASTCAM-SA1.1 675 K, Photron) attached to an upright microscope (Olympus 171, Japan) captures the images of the droplet at a rate of 500 fps and a size of 1024 × 1024 pixels. Stainless steel needles were used as fluidic interconnects. Unused ports were closed with solid needles. For the majority of our experiments, the flow rates of oil and water were fixed at 300 and 10 μl/h, respectively. The flow rates and their ratio make sure that only a single droplet at a time passages through the ten ratchets depicted in Fig. 1(a), and the droplet size is on the order of the ratchet size. The channels were flushed and cleaned carefully before a new set of liquid was used. The size and the velocity of the droplets were evaluated from the recorded images using a customized MATLAB program.

III. NUMERICAL METHOD

A. Numerical model and boundary conditions

We built a numerical model of the first two ratchets of the array based on the measured geometry of the test device [Fig. 1(b)]. The initial size of the droplet used in the simulation was taken from experimental data. The whole computational domain consists of a three-dimensional staggered uniform mesh. Due to symmetry, a one-quarter model as highlighted in Fig. 1(b) was considered. At the inlet, the carrier flow is fully developed with an average velocity of $\overline{u_c} = q_c/(wh)$, where q_c is the volumetric flow rate set by the syringe pump in the corresponding experiment and w and h are the channel width and height, respectively. Outflow boundary condition was used for the outlet. Symmetry boundary conditions are applied at $y=0$ μm and $z=0$ μm. As the channel wall is hydrophobic, there will be a thin film of oil between the water droplet and the wall. No-slip boundary condition was employed at the channel wall.

B. Mathematical formulation

The interface between the two liquids is traced with the level-set method [14]. The level-set function ϕ is used to define the interface Γ that separates water and oil. Its value is a signed normal distance function d from the interface,

$$\phi = \begin{cases} -d, & \vec{x} \in \Omega_c \\ 0, & \vec{x} \in \Gamma \\ +d, & \vec{x} \in \Omega_d, \end{cases} \quad (1)$$

where $\vec{x}$ is the location in the fluid Ω. The subscripts c and d refer to the continuous and the dispersed phases. The level-set function evolved as

$$\frac{\partial \phi}{\partial t} + \vec{u} \cdot \nabla \phi = 0. \quad (2)$$

The density ρ and the dynamic viscosity μ of the discontinuous liquid in the whole domain can be defined as

$$\rho = H\rho_d + (1 - H)\rho_c, \quad (3)$$

$$\mu = H\mu_d + (1-H)\mu_c. \qquad (4)$$

The smoothed Heaviside function H is expressed as

$$H(\phi) = \begin{cases} 0, & \phi < -\varepsilon \\ \dfrac{\phi+\varepsilon}{2\varepsilon} + \dfrac{1}{2\pi}\sin\left(\dfrac{\pi\phi}{\varepsilon}\right), & |\phi| \le \varepsilon \\ 1, & \phi > +\varepsilon, \end{cases} \qquad (5)$$

The parameter ε is set to 1.5 times of the control volume (CV) thickness in a uniform grid.

The continuity and momentum equations in Cartesian tensor notation for unsteady, viscous, incompressible, and immiscible two-phase systems are defined as

$$\frac{\partial \rho}{\partial t} + \nabla \cdot (\rho \vec{u}) = 0, \qquad (6)$$

$$\frac{\partial(\rho \vec{u})}{\partial t} + \nabla \cdot (\rho \vec{u}\vec{u}) = -\nabla p + \nabla \cdot \left[\mu(\nabla\vec{u} + \nabla\vec{u}^T)\right] + \vec{F}. \qquad (7)$$

In Eq. (7), $\vec{F}$ is the interfacial force

$$\vec{F} = -\sigma\kappa\hat{n}\delta(\vec{x} - \vec{x}_f), \qquad (8)$$

where σ is the interfacial tension, κ is the curvature, $\hat{n}$ is a normal to the interface, and $\delta(\vec{x}-\vec{x}_f)$ is the delta function that is zero everywhere except at the interface. These parameters are defined as

$$\hat{n}_F = \frac{\nabla(\phi)}{|\nabla(\phi)|},$$

$$\kappa = \nabla \cdot \hat{N}_F,$$

$$\delta(\vec{x} - \vec{x}_F) = D(\phi) = \begin{cases} \dfrac{1 + \cos(\pi\phi/\varepsilon)}{2\varepsilon}, & |\phi| < \varepsilon \\ 0, & \text{otherwise.} \end{cases} \qquad (9)$$

To maintain ϕ as a distance function, ϕ is set to the steady-state solution of the following equation:

$$\frac{\partial \phi'}{\partial \bar{t}} = \overline{\mathrm{sgn}}(\phi)(1 - |\nabla\phi'|), \qquad (10)$$

where $\bar{t}$ is a pseudotime for second level-set function ϕ' that is employed for redistancing purpose only, and $\overline{\mathrm{sgn}}(\phi)$ is given by

$$\overline{\mathrm{sgn}}(\phi) = \frac{\phi}{\sqrt{\phi^2 + |\nabla\phi|^2(\Delta x)^2}}. \qquad (11)$$

To reduce the mass loss problem, the particle correction procedure was implemented [13]. The governing equations (6) and (7) are solved on the staggered grid system by employing the finite volume method with SIMPLER algorithm [15]. The level-set and resistance functions are implemented to the narrow-band region near the interface instead of the whole computational domain [16]. Grid-independent study was carried out on the uniform grid in the nozzle direction. A mesh

(a) t=0 ms (b) t=18 ms
(c) t=30 ms (d) t=38 ms
(e) t=46 ms (f) t=54 ms
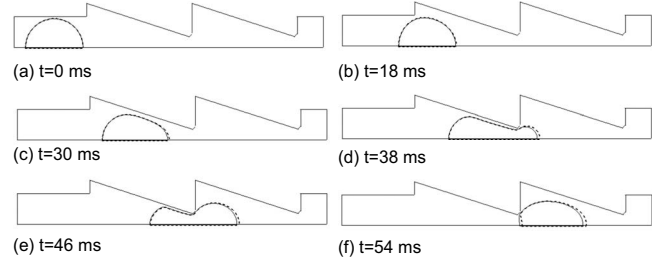
FIG. 2. Grid-independent study in nozzle direction (solid line: $227 \times 34 \times 18$ CVs at a time step of $\Delta t = 4 \times 10^{-5}$ s, dashed line: $354 \times 53 \times 27$ CVs with $\Delta t = 2 \times 10^{-5}$ s).

with $227 \times 34 \times 18$ control volumes and a time step of $\Delta t = 4 \times 10^{-5}$ s are sufficient to capture the droplet movement in our investigation.

C. Grid-independent study

A grid-independent study was carried out on the uniform grid in the nozzle direction (Fig. 2). The flow rate ratio between oil and water was set at 300 μl/h : 10 μl/h. The interfacial tension was set at the value of the surfactant concentration of 0.1% (w/w). Two different meshes with $227 \times 34 \times 18$ CVs at a time step of $\Delta t = 4 \times 10^{-5}$ s and $354 \times 53 \times 27$ CVs with $\Delta t = 2 \times 10^{-5}$ s were used. Figure 4 shows that the difference between the solutions is relatively small. Thus, the mesh $227 \times 34 \times 18$ CVs with $\Delta t = 4 \times 10^{-5}$ s is sufficient to capture the droplet movement through the microfluidic ratchets. This mesh density will be used in the numerical investigations reported in this paper.

IV. RESULTS AND DISCUSSION

In both simulation and experiment, the traveling distance of the advancing front of the droplet was measured. The velocity derived from this distance is thereafter referred to as the droplet velocity. Experimental and numerical results show that the droplet accelerates and decelerates during the passage in the test section (Fig. 3). The droplet always has a maximum velocity as it passes through the narrow necks. As shown in Figs. 1(c) and 1(d), the difference in radii of curvature between the advancing and receding ends of the droplet leads to an additional capillary force. Besides the factor caused by the sudden expansion or sudden constriction of the ratchet, the capillary force also affects the acceleration and deceleration processes. The capillary force is governed by the interfacial tension and the radii of curvatures at the advancing and receding surfaces.

To investigate the effect of viscosity on the droplet motion, we used a numerical model with fixed flow rates ($q_c = 300$ μl/h and $q_d = 10$ μl/h) and a fixed interfacial tension ($\sigma = 4.82$ mN/m). The properties of the liquids used in later experiments were taken as reference. At the same flow rates and at the same interfacial tension, the viscosity of the oil affects the droplet velocity significantly [Figs. 3(a) and 3(b)], while the viscosity of the droplet has a negligible effect [Figs. 3(c) and 3(d)]. The results also show that the acceleration and deceleration pattern depends on the ratchet
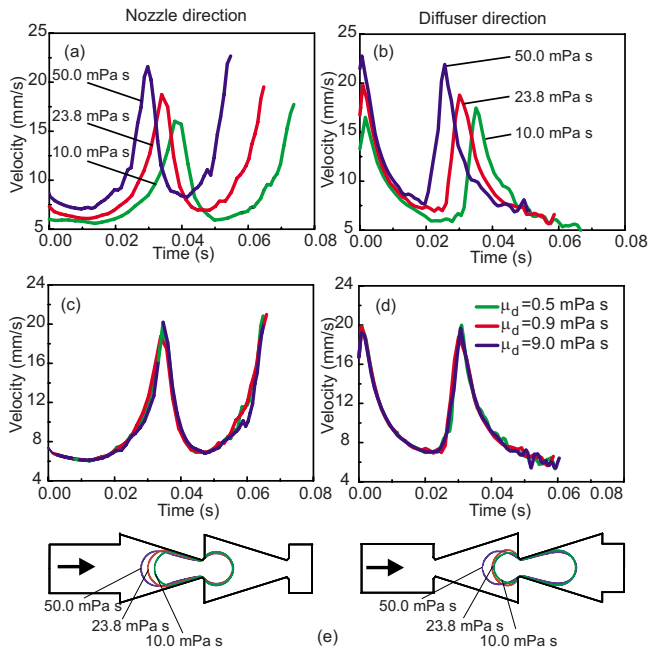
FIG. 3. (Color online) Simulated droplet velocities at different viscosities of the continues phase in (a) nozzle and (b) diffuser directions, as well as of the disperse phase in (c) nozzle and (d) diffuser directions. (e) The higher viscosity of the continuous phase squeezes and elongates the droplet leading to a large difference in radius of curvature between the advancing receding surfaces. (q_c =300 μl/h, q_d=10 μl/h, and σ=4.82 mN/m).

direction. The acceleration and deceleration are approximately symmetric about the maximum velocity in the nozzle direction, but asymmetric in the diffuser direction. A droplet of the same size, of the same interfacial tension, and of the same viscosity moves faster in a more viscous continuous phase. The higher viscosity of the continuous phase squeezes and elongates the droplet leading to a large difference in radius of curvature between the advancing receding surfaces [Fig. 3(e)]. Thus, the capillary force acting on the droplet is higher with a higher viscosity of the continuous phase.

Next, we tested the effect of droplet size both numerically and experimentally. As the droplet size is affected by the interfacial tension, we design a control experiment to discriminate the effect of droplet size on the motion. The experiment only considers oil with 0.5% (w/w) surfactant. The total flow rate was kept at 310 μl/h so that the average mean velocity remains constant. The droplet size was changed by varying the flow rate ratio between oil and water. Both numerical and experimental results indicate that the droplet velocity is not significantly affected by the droplet size [Figs. 4(a)–4(d)]. The tested range of droplet size is approximately the range caused by the different interfacial tensions in our subsequent experiment.

In the last experiment, we varied the interfacial tension with different surfactant concentrations. As measured before, the viscosity of the oil remains unchanged. The key observation in this experiment is that droplets with a higher surfactant concentration or a lower interfacial tension always move faster in both directions [Figs. 5(a) and 5(c)]. Although the experimental and numerical results show the same trends,
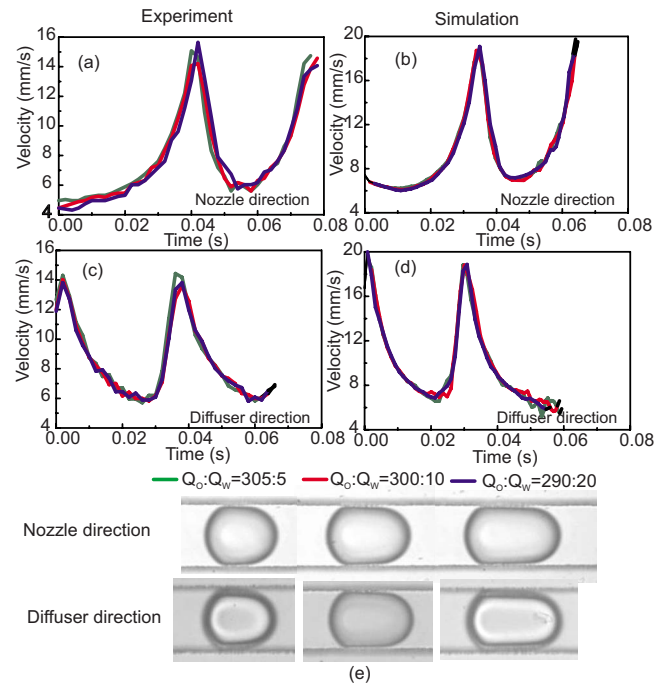
FIG. 4. (Color online) The effect of different droplet sizes on the droplet velocities: (a) experimental data for nozzle direction; (b) numerical data for nozzle direction; (c) experimental data for diffuser direction; (d) numerical data for diffuser direction; (e) formed droplets at different flow rate ratios in both directions.

their magnitudes are slightly different [Figs. 5(b) and 5(d)]. The discrepancy of about 20% could be caused by the trapezoid cross section of the fabricated microchannel. The numerical model only considers a rectangular cross section and the first two in the array of the ten ratchets.

For the convenience of generalization of the results, the effect of the viscosity of the carrier fluid and the interfacial
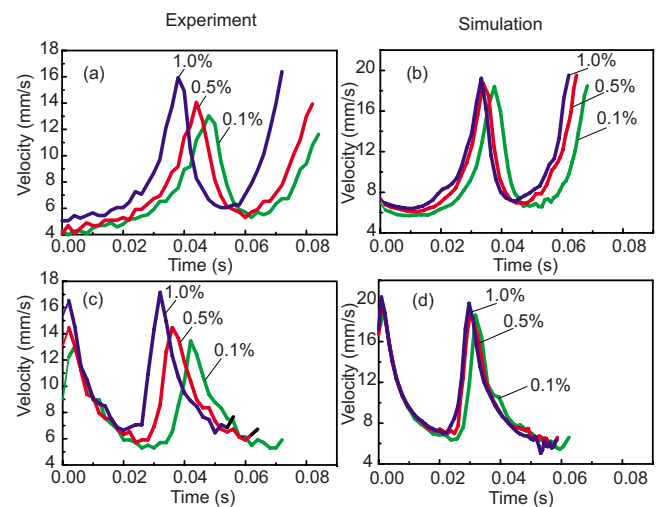
FIG. 5. (Color online) The effect of different surfactant concentrations or different interfacial tensions on the droplet velocities: (a) experimental data for nozzle direction; (b) numerical data for nozzle direction; (c) experimental data for diffuser direction; (d) numerical data for diffuser direction.
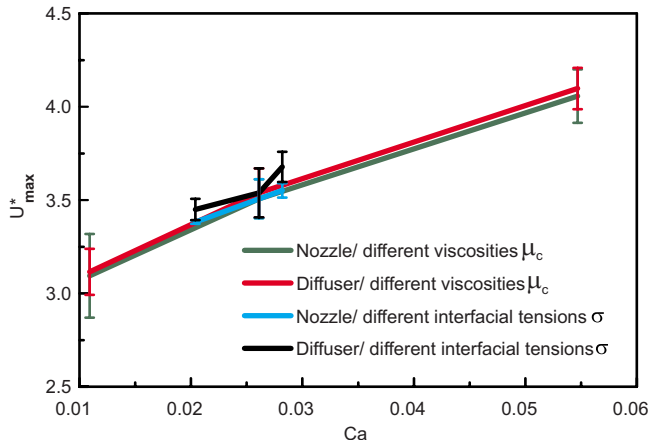
FIG. 6. (Color online) Dimensionless maximum velocity of the droplet as a function of capillary number.

tension is represented by the capillary number $Ca = \bar{u}_c \mu_c / \gamma$. The droplet diameter is normalized by the channel width w and the droplet velocity is normalized by the mean velocity of the continuous phase $\bar{u}_c$. Figure 6 shows the simulated droplet velocity $U_{max}^* = U_{max} / \bar{u}_c$ as a function of the capillary number Ca. Although the results were obtained by varying the dynamic viscosity of the continuous phase or by varying the interfacial tension, the same trends of the maximum droplet velocity is observed. At a given mean velocity (fixed flow rates), the maximum droplet velocity increases with increasing capillary number. The velocity in the diffuser direction is higher than that in the nozzle direction.

Figure 7 shows the experimental results of the droplet size and the maximum droplet velocities functions of the capillary number. The capillary number was varied by changing the interfacial tensions with different surfactant concentrations. The higher capillary number leads to a smaller droplet formed at the T junction of the test devices [Fig. 7(a)]. The results also indicate that a lower interfacial tension or a higher capillary number makes the droplet moves faster in both directions of the ratchet [Fig. 7(b)]. This trend agrees well with the results predicted by numerical simulation (Fig. 6). However, for the same range of capillary number the measured velocity is slightly lower than the simulated one. The discrepancy could be explained by the simplified numerical model. For the range of droplet size considered in the experiment, the velocity is independent of the droplet size (Fig. 4). Thus, the magnitude of interfacial tension is the single parameter that determines the droplet velocity. Thus, measuring the droplet velocity can determine the interfacial tension. The difference in magnitudes of droplet velocity in both directions indicates that the ratchets exhibit rectification characteristics that can be used for designing micropumps for delivering multiphase systems such as a droplet train.

V. CONCLUDING REMARKS

In conclusion, we present an important observation that for a limited range of capillary number the droplet velocity
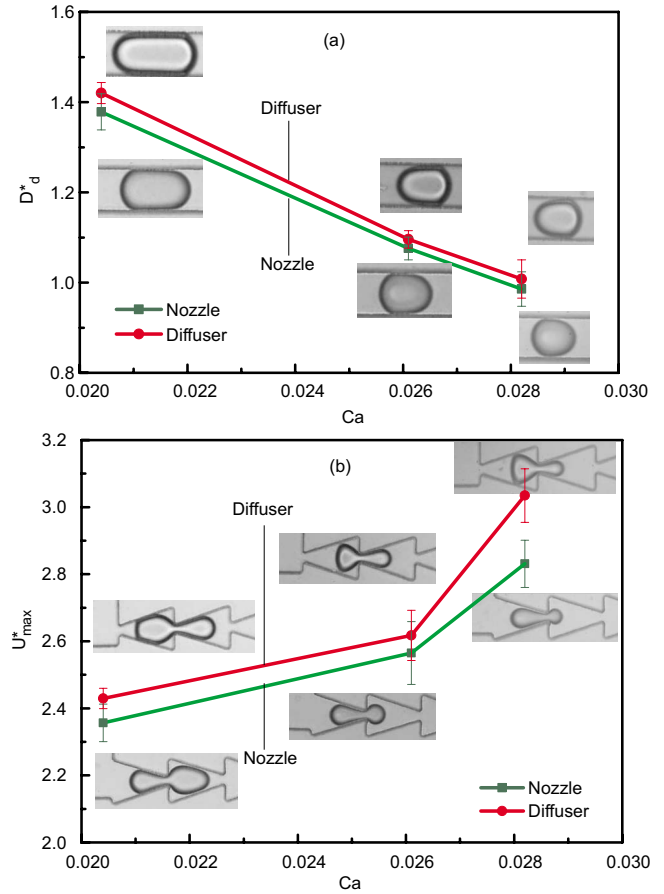
FIG. 7. (Color online) The effect of capillary number on the (a) droplet size and (b) its velocity (flow rate ratio between oil and water is kept constant at 300 μl/h:10 μl/h).

in an array of microfluidic ratchets is a function of interfacial tension and independent of both the droplets size and the viscosity of the droplet liquid. Densities of the liquid are insignificant because gravitational forces are negligible in the microscale. Mineral oils with different concentrations of surfactant Span 80 was tested at constant flow rates of oil and water. A lower interfacial tension results in a smaller droplet size and increases the droplet velocity. The same phenomena were observed with a three-dimensional numerical model. Although only two ratchets are modeled in the simulation, numerical results agree relatively well with experimental data. The results presented here show possibilities of measuring interfacial tension and designing micropumps for multiphase systems.

[1] M. Srisa-art, A. J. deMello, and J. B. Edel, Phys. Rev. Lett. **101**, 014502 (2008).

[2] U. Lehmann, S. Hadjidj, V. K. Parashar, C. Vandevyver, A. Rida, and M. A. M. Gijs, Sens. Actuators B **117**, 457 (2006).

[3] H. Song, D. L. Chen, and R. R. Ismagilov, Angew. Chem., Int. Ed. **45**, 7336 (2006).

[4] T. Thorsen, R. W. Roberts, F. H. Arnold, and S. R. Quake, Phys. Rev. Lett. **86**, 4163 (2001).

[5] P. Garstecki, M. J. Fuerstman, H. A. Stone, and G. M. Whitesides, Lab Chip **6**, 437 (2006).

[6] N. Pannacci, H. Bruss, D. Bartolo, I. Etchart, T. Lockhart, Y. Hennequin, H. Willaime, and P. Tabeling, Phys. Rev. Lett. **101**, 164502 (2008).

[7] J. H. Xu, S. W. Li, W. J. Lan, and G. S. Luo, Langmuir **24**, 11287 (2008).

[8] N. T. Nguyen, T. H. Ting, Y. F. Yap, T. N. Wong, J. C. K. Chai, W. L. Ong, J. L. Zhou, S. H. Tan, and L. Yobas, Appl. Phys. Lett. **91**, 084102 (2007).

[9] N. T. Nguyen, S. Lassemono, F. A. Chollet, and C. Yang, IEEE Sens. J. **7**, 692 (2007).

[10] N. T. Nguyen, S. Lassemono, F. A. Chollet, and C. Yang, IEE Proc.: Nanobiotechnol. **153**, 102 (2006).

[11] J. T. Cabral and S. D. Hudson, Lab Chip **6**, 427 (2006).

[12] N. T. Nguyen, S. Lassemono, and F. A. Chollet, Sens. Actuators B **117**, 431 (2006).

[13] N. T. Nguyen, Y. C. Lam, S. S. Ho, and C. L. N. Low, Biomicrofluidics **2**, 034101 (2008).

[14] S. Osher and J. A. J. Sethian, J. Comput. Phys. **79**, 12 (1988).

[15] S. V. Patankar, *Numerical Heat Transfer and Fluid Flow* (Hemisphere Publisher, New York, 1980).

[16] D. Peng, B. Merriman, S. Osher, H. Zhao, and M. Kang, J. Comput. Phys. **155**, 410 (1999).